



Effect of high-energy ball milling on the electrical properties of NaTaO₃ ceramic

Uttam K. Mahto¹, Sumit K. Roy², Kumar AmarNath³, Kamal Prasad^{1,4,*}

¹Aryabhatta Centre for Nanoscience and Nanotechnology, Aryabhatta Knowledge University, Patna 800001, India

²Department of Physics, St. Xavier's College, Ranchi 834001, India

³HEG Ltd., Mandideep, Raisen 462046, India

⁴University Department of Physics, T.M. Bhagalpur University, Bhagalpur 812 007, India

Received 7 May 2016; Received in revised form 25 August 2016; Accepted 6 September 2016

Abstract

In this work, the effect of high energy milling time on the structural and electrical properties of NaTaO₃ (NT) ceramics synthesized using standard solid-state reaction method was investigated. X-ray diffraction studies indicated that the unit cell structure for all samples is orthorhombic (space group: Pnma). FTIR spectra also confirmed the formation of NT without any new phase. The NT ceramics prepared with 10 h milled powder showed the formation of small grain sizes (~1.2 μm) which is beneficial for dielectric applications in high density integrated devices. The NT ceramics prepared with the 10 h milled powder exhibited superior dielectric properties, i.e. enhancement in ε' value (from 290 to 1270) and reduction in tg δ (from 0.59 to 0.23) at 1 kHz compared to the ceramics prepared with the unmilled powder. Impedance analysis indicated the negative temperature coefficient of resistance (NTCR) character with non-Debye type of dielectric relaxation. The correlated barrier hopping model successfully explains the mechanism of charge transport in the present ceramic samples. The values of remnant polarization and coercive field of the poled samples prepared with the unmilled and 10 h milled powders were found to be 0.71 μC/cm² and 2.03 kV/cm and 8.74 μC/cm² and 4.14 kV/cm, respectively. The field dependent polarization studies at room temperature indicated that NT is a promising lead-free electrostrictive material for industrial applications.

Keywords: NaTaO₃, lead-free electroceramics, milling, structure, dielectric and ferroelectric properties

I. Introduction

Perovskite-type materials with ABO₃ structure have been widely used in different electronic and microelectronic devices, such as capacitors, piezoelectric transducers, pyroelectric detectors/sensors, memory devices, microwave tunable devices, electrostrictive actuators, SAW substrates, MEMS, etc. It is observed that materials used for most of these applications are made from lead bearing compounds, such as lead titanate, lead zirconate titanate, lead magnesium niobates, etc. In recent years, efforts are being made worldwide to improve the performance characteristics of lead-free ABO₃-type

materials which can find their applications in such electronic/microelectronic devices [1–15]. Among them, NaTaO₃ is a well-known perovskite oxide which is considered to be a feasible alternative to commercially available Pb-based piezoceramics [13,16,17]. Further, development of new lead-free materials with microelectronic technologies, leading to higher efficiency and miniaturization have opened up scope for the development of highly integrated devices. To this end, materials having large grain sizes (> 2 μm) and high dissipation factor possess difficulty in developing a dielectric layer less than 10 μm with higher capacitance values [18]. Besides, according to several reports improvement on the physical, electrical and piezoelectric properties of the ceramics synthesized from the nanocrystalline powders have been noticed [19,20]. An important aspect for im-

*Corresponding author: tel: +91 612 2351919,
fax: +91 612 2351911, e-mail: k.prasad65@gmail.com,
k_prasad65@yahoo.co.in

proving the sinterability of NT ceramic is the reduction in initial particle size, due to the fact that the driving force for sintering is inversely proportional to the particle size [21]. There are several methods available for the synthesis of nanostructured materials such as: high energy ball milling, solvothermal, hydrothermal, microemulsion as well as different chemical routes. However, each method has its own advantages and disadvantages like high energy consumption, expensive chemicals, long processing time, generation of toxic wastes, etc. The high-energy ball milling technique is still considered as a simple and cost effective method for large scale production of nanoceramic powders. It has been found that high energy milling is an effective way to modify the morphology, reduce the particle size and consequently enhance the densification of nanoceramic powders. Also, an extensive literature survey suggested that no attempt, to the authors' knowledge, has so far been made to study high energy ball milled perovskite NaTaO₃ ceramics. However, there is quite a few report available on the formation of nanoscale NaTaO₃ ceramics using mechanochemical synthesis using the constituent chemicals Na₂CO₃ and Ta₂O₅ [22].

Accordingly, in the present work, NaTaO₃ (NT) ceramic samples were prepared by a standard solid state reaction technique (industrially viable method) and fine powders were obtained using high energy ball milling method. The obtained NT ceramics were characterized using X-ray diffraction, SEM, IR spectroscopy, dielectric, impedance and AC conductivity studies.

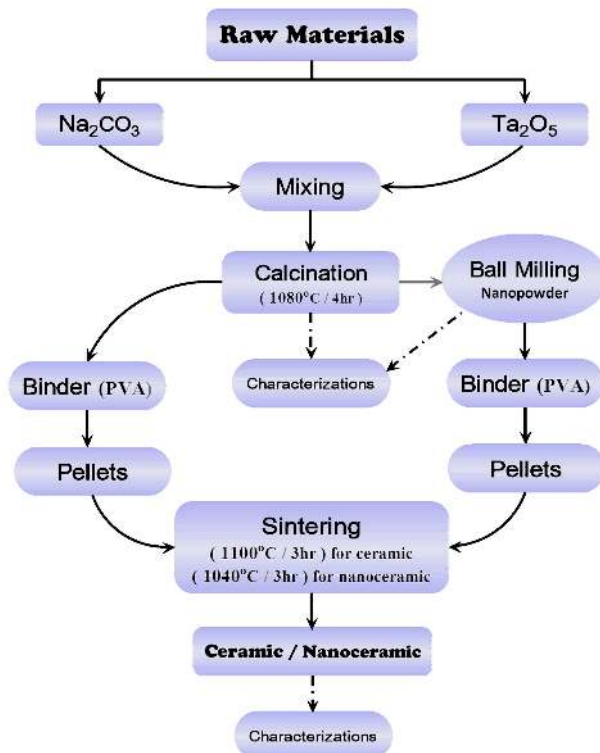


Figure 1. Schematics for synthesis of NaTaO₃ ceramics using high energy ball milling method

II. Materials and methods

2.1. Preparation of NT ceramic samples

The polycrystalline NaTaO₃ samples were prepared by the standard solid-state reaction technique and a high energy ball milling technique (Fig. 1). High purity (>99.9%) Na₂CO₃ (Merck, Germany) and Ta₂O₅ (Aldrich, USA) were mixed in proper stoichiometric ratios. Wet mixing was carried out with acetone as the medium for homogeneous mixing. The well-mixed powder was then calcined at 1080 °C for 4 h. The completion of reaction and the formation of desired compound were checked by X-ray diffraction technique. The as-calcined powder was high-energy milled in isopropanol medium using water cooled bench top planetary ball mill type grinding machine (Emax, Retsch, Germany). The milled powders were taken out at different milling time, i.e. 0, 2.5, 5, 7.5 and 10 h, for their structural and IR analyses and denoted as NT-0, NT-2.5, NT-5, NT-7.5 and NT-10, respectively. Further, the calcined powders (unmilled and milled for 10 h) were compacted into thin (~1.25 mm) circular disks with an applied uniaxial pressure of 650 MPa. The NT-0 (prepared with the unmilled powder) and NT-10 (prepared with the 10 h milled powder) pellets were sintered in air at 1100 °C/3 h and 1040 °C/2 h, respectively.

2.2. Characterizations

The XRD data of the unmilled and milled (2.5, 5, 7.5 and 10 h) powders were obtained by X-ray diffractometer (XPERT-PRO, Pan Analytical, USA) at room temperature, using CuK_α radiation ($\lambda = 1.5405 \text{ \AA}$) over a wide range of Bragg angles ($20^\circ \leq 2\theta \leq 70^\circ$). The Fourier transformed infrared (FTIR) spectra of all samples were collected in the transmission mode using an Alpha-T Bruker FTIR spectrophotometer in the range of 500–5000 cm⁻¹. The scanning electron micrographs (SEM) of fractured surface of the NT-0 and NT-10 ceramics were recorded using SEM JEOL-JSM840A, Japan. The density of the sintered pellets was determined by the Archimedes method. Dielectric and impedance measurements were carried out as function of frequency (20 Hz–10 MHz) at different temperatures (20–500 °C) using a computer-interfaced Impedance analyser (E4990A-120, Keysight Technologies, USA). Symmetrical Ag|Ceramic|Ag cells, where Ag is a conductive paste (Ted Pele, USA) coated on both sides of the pellets, were prepared for the measurements. AC conductivity data were obtained using the following relation:

$$\sigma_{ac} = 2\pi \cdot f \cdot \epsilon_0 \cdot \epsilon'' \quad (1)$$

where f is the operating frequency, $\epsilon_0 = 8.85 \times 10^{-12} \text{ F/m}$ is the permittivity of the free space and ϵ'' imaginary part of permittivity. The field dependent polarization (P) curves for the poled samples at room temperature were obtained using an Advanced Piezo Tester (PMF1114-371, Radiant Technologies Inc., USA). The samples

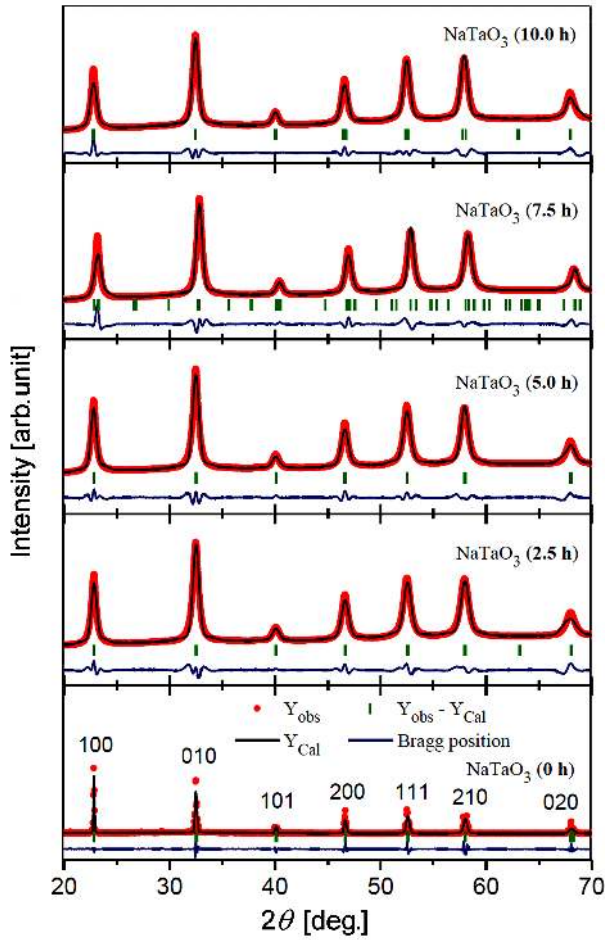


Figure 2. XRD patterns of NaTaO₃ ceramic powders prepared with different milling times

were poled in silicone oil at 25 °C under an electric field of 2.5 kV/mm for 15 min.

III. Results and discussion

3.1. Microstructural characterization

X-ray diffraction patterns of the unmilled and milled (2.5, 5, 7.5 and 10 h) NT ceramic powders along with their Rietveld refinement profiles are shown in Fig. 2. All XRD data show a single orthorhombic phase formation with space group *Pnma*. The refined unit cell parameters are listed in Table 1. No significant change in the unit cell parameters were observed as the values are almost same. However, the broadening in the XRD peaks could be seen which clearly indicates the particle

size reduction of NT while undergone milling. Further, apparent particle sizes and lattice strain values were obtained from linear least square fitting of $B \cos \theta - \sin \theta$ data to Williamson-Hall equation:

$$B \cos \theta = (K\lambda/D) + 2(\Delta\xi/\xi) \sin \theta \quad (2)$$

where B is diffraction peak width at half intensity, $\Delta\xi/\xi$ is the lattice strain, K is the Scherrer constant (0.89) and the term $K\lambda/D$ represents the Scherrer particle size distribution. A reduction in the value of apparent particle size from 216 nm for the unmilled sample to 70 nm for the 10 h milled one was observed, while the milling resulted in the increase in the value of lattice strain from 0.06 to 0.19, respectively.

Figure 3 shows SEM micrographs of the fractured surfaces of the sintered ceramics NT-0 and NT-10. The micrographs clearly exhibit that the grains become finer (the average grain size decreases from ~2.5 μm to ~1.2 μm) and their distribution becomes more homogeneous with fewer pores when the NT powder was milled for 10 h. This may be due to the reduction in particle sizes which might have produced some stress during high energy milling. This generated stress could prevent grain boundary movement during the sintering and thereby resulted in the reduction of grain size. Besides, it could be noted that a lower sintering temperature/time was required compared to the NT-0 ceramics which is also lower than the calcination temperature/time as well. This could be due to lowering of particle as well as grain sizes of the NT-10 ceramics. The variation of experimentally determined ceramic density with milling time is shown in Fig. 3b. It is observed that the ceramic density appreciably increase with milling time from 89.6% (for the NT-0 sample) to 92.8% (for the NT-10 sample) of the theoretical density.

Figure 4 depicts the FTIR spectra of all samples in the mid infrared region. A prominent peak at 654 cm⁻¹ can be observed and corresponds to the Ta–O bond thereby confirming the formation of desired perovskite phase compound [23]. The investigated samples also contain the multiple peaks (A–O absorption bands) in the frequency region 1000–1405 cm⁻¹, which are due to the presence of Na–O vibrations [24,25]. All samples contain weak band at 2848–2928 cm⁻¹ which corresponds to carbonate groups, may be due to atmospheric CO₂. Further, the bands at 1646 cm⁻¹ and 3435 cm⁻¹ are assigned to the bending of O–H–O and O–H stretching modes of vibration due to physically adsorbed water molecules on

Table 1. Crystal data and refinement factors of NaTaO₃ (prepared using different milling time: 0, 2.5, 5.0, 7.5 and 10 h) obtained from X-ray powder diffraction data

Parameters	NT-0	NT-2.5	NT-5	NT-7.5	NT-10
Crystal system	Orthorhombic	Orthorhombic	Orthorhombic	Orthorhombic	Orthorhombic
Space group	<i>Pnma</i>	<i>Pnma</i>	<i>Pnma</i>	<i>Pnma</i>	<i>Pnma</i>
<i>a</i> [Å]	5.5241	5.535	5.534	5.529	5.531
<i>b</i> [Å]	7.7929	7.8025	7.705	7.795	7.8
<i>c</i> [Å]	5.4792	5.4811	5.481	5.481	5.481
<i>V</i> [Å ³]	235.8747	236.672	236.45	236.23	236.42

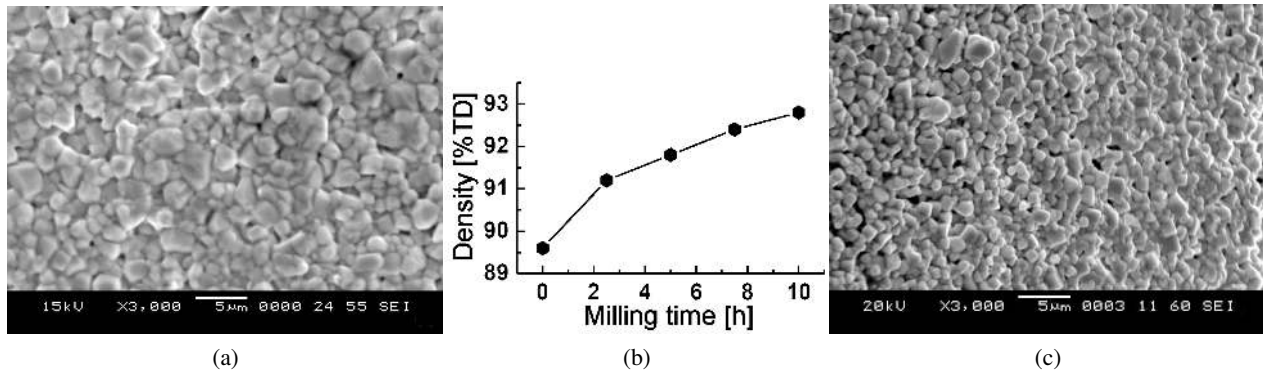


Figure 3. SEM images of fractured surface of NaTaO₃ ceramics – NT-0 (a) and NT-10 (c), and variation of ceramic density with milling time (b)

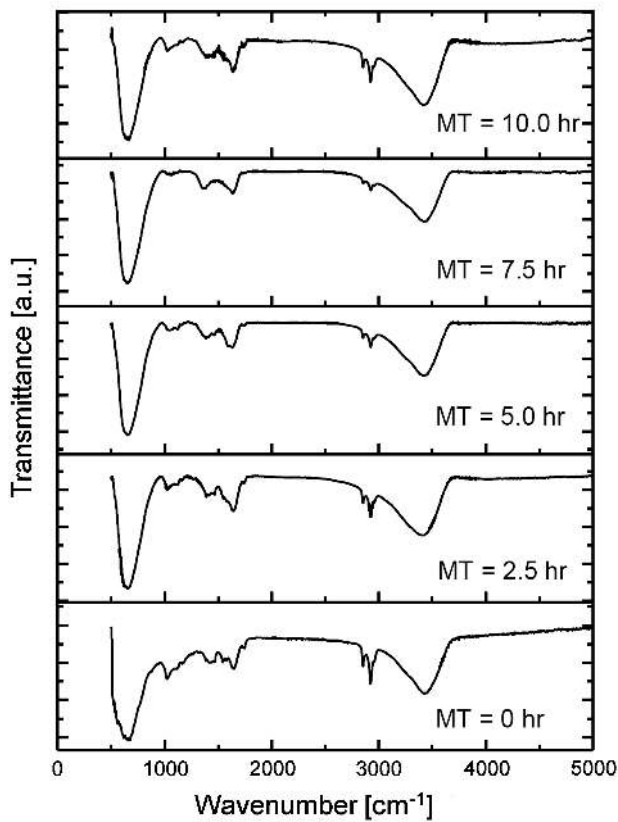


Figure 4. FTIR spectra of NaTaO₃ ceramic powders at different milling times

the sample surface during palletisation with KBr [26,27] and can be seen in all powders. No significant change in the IR spectra was observed due to increase of milling time.

3.2. Dielectric properties

The frequency response of the real, ϵ' , and imaginary, ϵ'' , parts of permittivity data at different temperatures, for the samples NT-0 and NT-10 are shown in Fig. 5. It is observed that both ϵ' and ϵ'' follow inverse dependence on frequency for both NT ceramics which is due to the fact that dipoles can no longer follow the field at high frequencies. Besides, it is observed that a peak starts appearing in the $\epsilon'' - f$ plots which shifts to

higher frequencies when temperature is increased with a decrease in its amplitude (Fig. 5).

The temperature dependence of ϵ' and ϵ'' at different frequencies for the NT-0 and NT-10 ceramic samples were shown in Figs. 6a and 6b, respectively. It is seen that the value of ϵ' first decreases up to $\sim 150^\circ\text{C}$ and $\sim 200^\circ\text{C}$ for the NT-0 and NT-10 samples respectively, which probably due to the ferroelectric phase transition at lower temperature. At higher temperature the ϵ' increases. The $\epsilon'' - T$ curves show a peak which shifts toward lower temperatures with increasing frequency in case of the NT-0 sample while no such peak was observed in case of the NT-10 sample. The values of ϵ' and ϵ'' at 25°C and 1 kHz are 290 and 172 for the NT-0 and 1270 and 287 for the NT-10 ceramic samples. The reason for the high dielectric constant could be considered due to the grain-boundary and/or the grain-size dependent extrinsic factors as well as a significant contribution of the intrinsic factors related to chemical substitution induced localized electronic structure modifications might plays a crucial role. Hence, the NT-10 ceramic sample exhibits superior dielectric properties (enhancement in ϵ' -value and reduction in $\text{tg } \delta (= \epsilon''/\epsilon' = 0.23)$ value) compared to the NT-0 one. Therefore, the NT-10 ceramics with small grain sizes ($< 1.2 \mu\text{m}$) could be considered as a potential lead-free candidate for dielectric applications in high density integrated devices.

The logarithmic frequency dependence of real (Z') and imaginary (Z'') parts of impedance of the samples NT-0 and NT-10, at different temperatures are plotted in Figs. 7a and 7b, respectively. It is observed that the value of Z' decreases with increasing frequency temperature for both samples and confirming the negative temperature coefficient of resistance (NTCR) character of NT ceramics. Further, at lower temperatures, the values of Z'' decrease monotonically suggesting the absence of any relaxation. This suggests that the relaxation species are immobile defects and the orientation effect might be associated. As the temperature increases, the peak in $Z'' - f$ plots appears, which shifts towards higher frequency with the increment in temperature showing the resistance is decreasing and supports NTCR character of the NT-0 and NT-10 ceramics. Further, the magni-

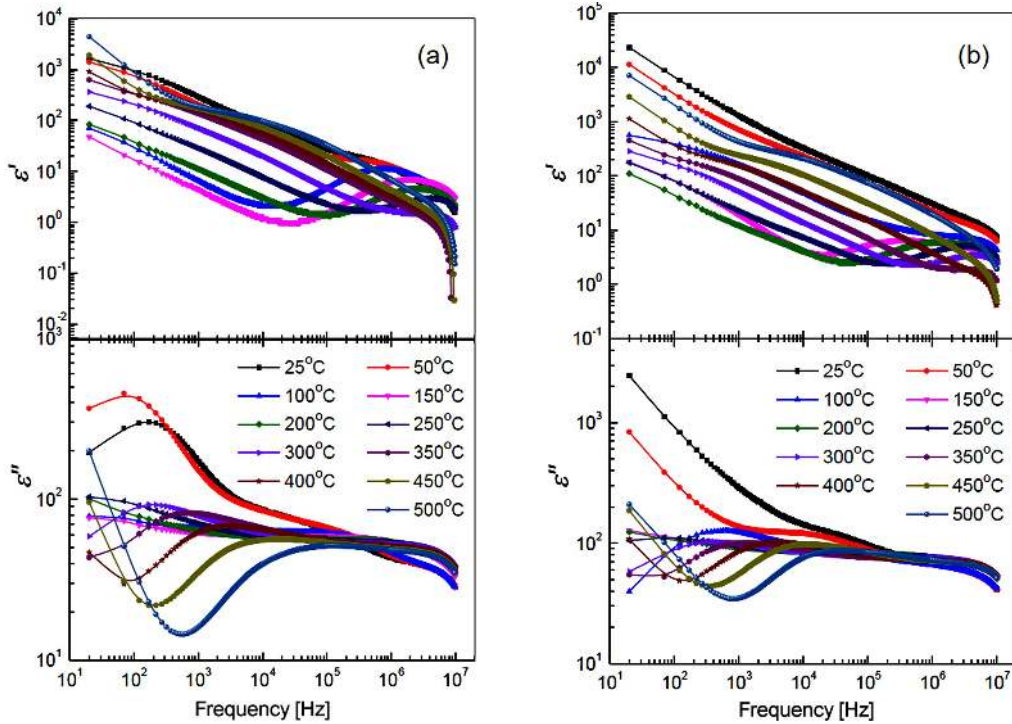


Figure 5. Frequency dependence of real and imaginary parts of dielectric constant of: a) NT-0 and b) NT-10 NaTaO₃ ceramics at different temperatures

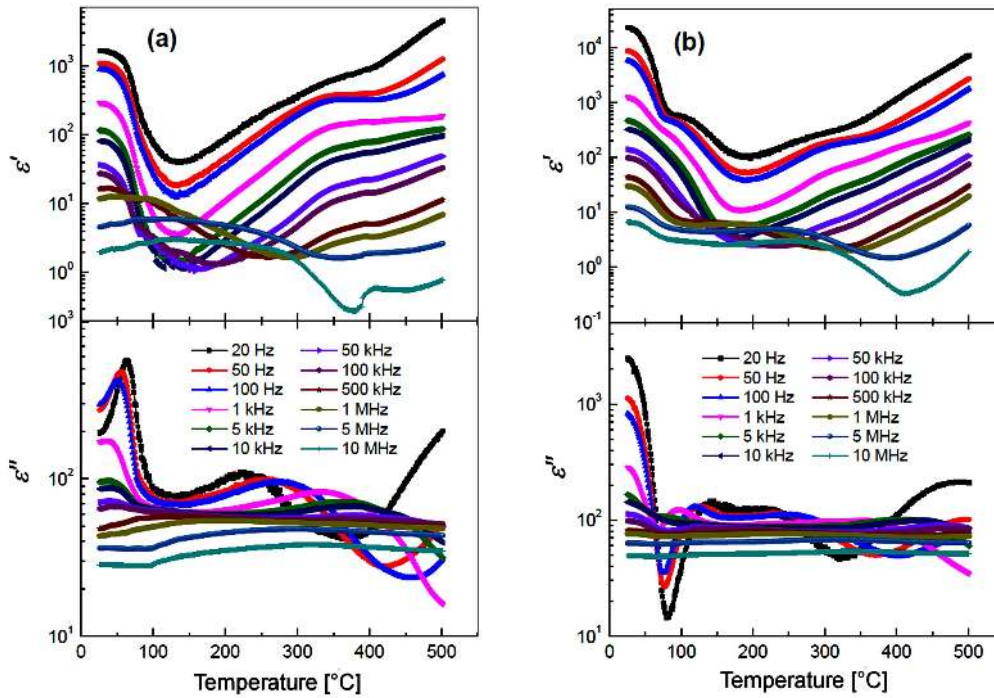


Figure 6. Temperature dependence of real and imaginary parts of dielectric constant of: a) NT-0 and b) NT-10 NaTaO₃ ceramic samples at different frequencies

tude of Z'' peaks decreases while the width of the peak increases with increasing temperature and the peaks are slightly asymmetric in nature for both samples, which suggests that there is a spread of relaxation times i.e. the existence of a temperature dependent electrical relaxation in the materials [28]. As shown in insets of Fig. 7, a depressed semicircular arc is seen in the complex

plane plot corresponding to a temperature of 500 °C. It can be seen that the centres of both semicircular arcs lie below the x-axis, thereby indicating non-Debye type relaxation process in NT ceramics.

In polycrystalline materials, impedance formalism emphasizes grain boundary conduction process, while bulk effects on frequency domain dominate in the elec-

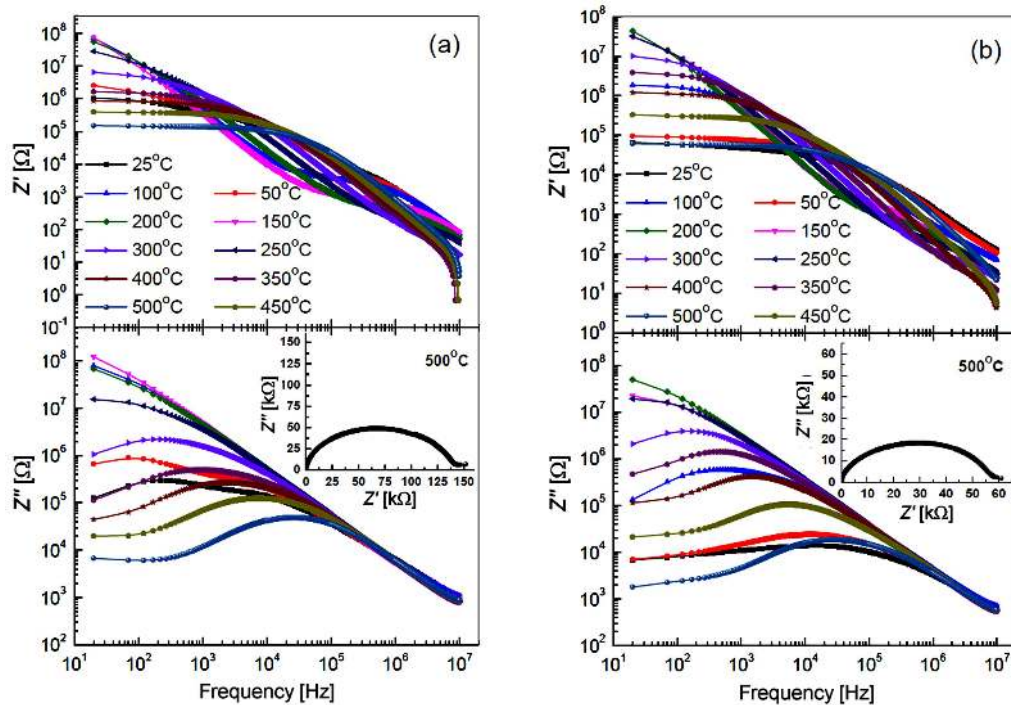


Figure 7. Frequency dependence of real and imaginary parts of impedance of: a) NT-0 and b) NT-10 NaTaO₃ ceramic samples at different temperatures. Inset: Cole-Cole plot at 500 °C

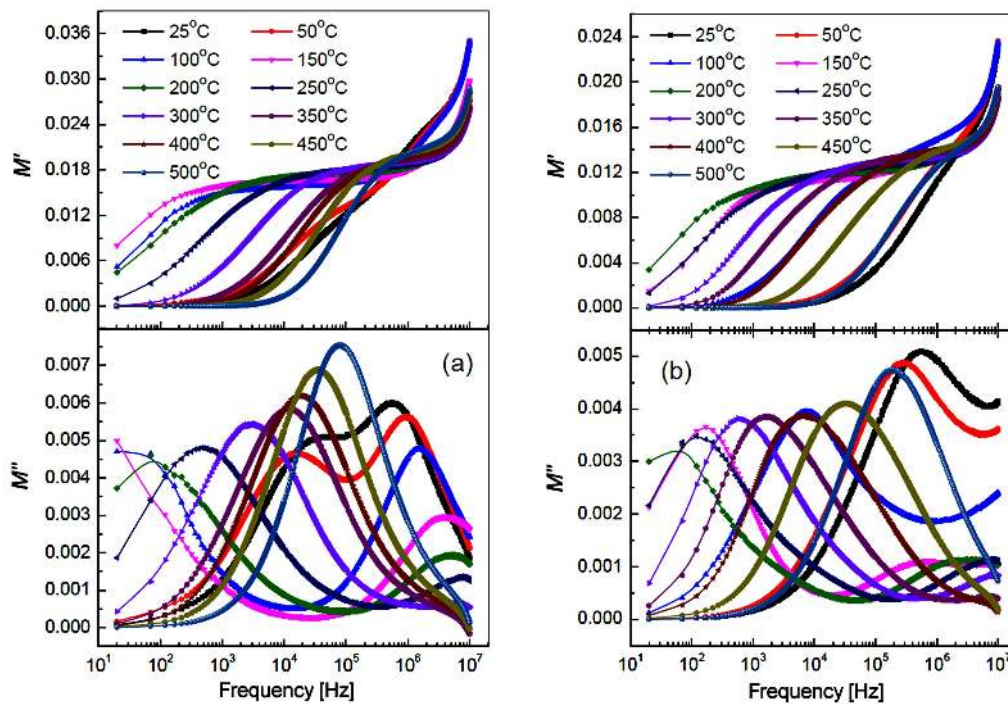


Figure 8. Frequency dependence of real and imaginary parts of electric modulus of: a) NT-0 and b) NT-10 NaTaO₃ ceramic samples at different temperatures

tric modulus formalism. The use of modulus spectroscopy plot is particularly useful for separating the components with similar resistance but different capacitance. The other advantage of electric modulus formalism is that the electrode effect is suppressed. Due to the above reasons, complex electric modulus formalism was also adopted in the present case in order to see the differ-

ent effects separately. Dielectric relaxation studies were carried out in the complex modulus M^* formalism. The variation of real (M') and imaginary (M'') parts of electric modulus with frequency for the NT-0 and NT-10 ceramics at different temperatures are shown in Figs. 8a and 8b, respectively. They are characterized by very low value (\sim zero) of M' in the low frequency region and a

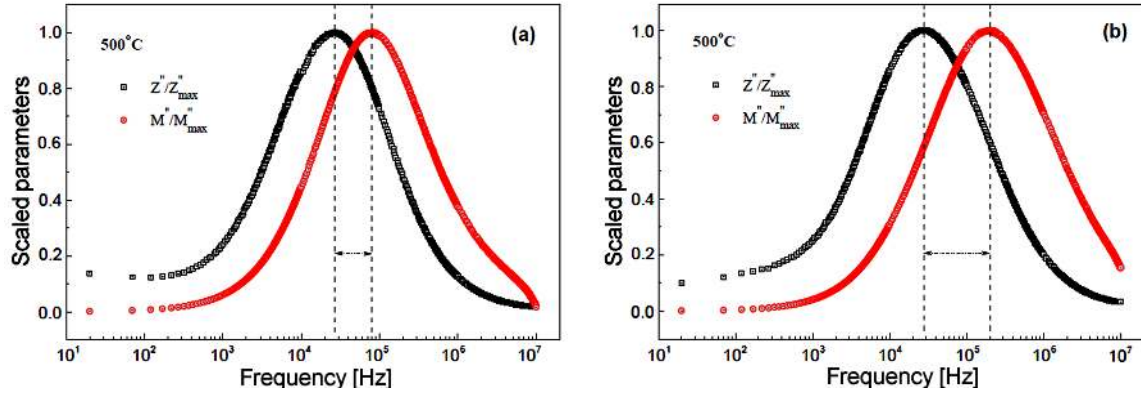


Figure 9. Variation of normalized Z'' and M'' with frequency of: a) NT-0 and b) NT-10 NaTaO_3 at 500°C

sigmoidal increase in the value of M' with the frequency approaching ultimately to M_∞ . This can be attributed to the conduction phenomena due to short range mobility of charge carriers. Also, the value of which (M'), increases with the increment in frequency after 1 MHz. The variation of M'' with frequency at different temperatures are characterized by: i) clearly resolved peaks in the pattern appearing at unique frequency at different temperatures, ii) significant asymmetry in the peak with their positions lying in the dispersion region of M' vs. frequency pattern and iii) the peak position shifts towards higher frequency side with rise in temperature. At lower frequencies, charge carriers can move freely to a longer distance (i.e. ions can perform successful hopping from one site to another executing long-range mobility) up to a certain frequency (frequency maximum). Further increase in the frequency leads to the formation of localized sites, which can trap the carriers. Therefore, displacement of carriers which move within the sample by discrete hops between randomly distributed localized sites (i.e. short-range motion). Therefore, the region where peak occurs is an indicative of the transition from long-range to short-range mobility with increase in frequency [29,30]. This behaviour suggests that the spectral intensity of the dielectric relaxation is activated thermally in which hopping process of charge carriers and small polarons dominate intrinsically. Both the electric modulus and the impedance formalism produces peaks in their frequency spectrum, which are broader than as predicted by Debye theory of relaxation phenomena and are significantly asymmetric. Furthermore, the appearance of peak in modulus spectrum provides a clear indication of conductivity relaxation. Also, M'' peak gets broadened upon increasing temperature suggesting an increase in non-Debye behaviour [31]. This particular behaviour seems to be unique to electrical relaxation since all other relaxation processes (e.g. mechanical, light scattering) typically exhibit opposite behaviour with tendency towards Debye behaviour with increasing temperature [26]. According to ideal Debye theory of relaxation the impedance and modulus maxima are supposed to appear at the same frequency at a temperature, which are not observed for the studied

compounds. Besides, the values of M' are observed to be lower in the case of the NT-10 ceramics.

The variations of scaled parameters (Z''/Z''_{max} and M''/M''_{max}) with frequency of the NT-0 and NT-10 ceramics at 500°C are shown in Figs. 9a and 9b, respectively. It is observed that the peaks are not occurring at the same frequency rather following the sequence: $f_{Z''} < f_{M''}$. The magnitude of mismatch between the peaks (Δf) of these parameters represents a change in the apparent polarization. The overlapping of peaks is an evidence of long-range conductivity whereas the difference is an indicative of short-range conductivity (via hopping type of mechanism) [32]. Also, the value of Δf increases in the case of the sample NT-10 which simply supports that the short-range conductivity via hopping type of mechanism.

3.3. Conductivity

The log-log plots of AC electrical conductivity with frequency for the NT-0 and NT-10 ceramics at different temperatures are shown in Figs. 10a and 10b, respectively. The AC conductivity spectrum for both samples show dispersion throughout the chosen frequency range and with the increment in temperature plots get flattened (plateau value). The switch from the frequency-independent to the dependent regions shows the onset of the conductivity relaxation phenomenon which indicates the translation from long range hopping to the short range ion-motion [33]. This observation can be well expressed by the Jonscher's universal power law:

$$\sigma_{AC} = \sigma_{DC} + A\omega^s \quad (3)$$

where σ_{DC} is the frequency independent (DC) part of conductivity [34]. The second term in the right hand side is the frequency sensitive region with $0 \leq s \leq 1$. It was found that the value of index s decreases with the rise of temperature and is always less than 1. The model based on hopping of charge carriers can be expressed with the following equation:

$$s = 1 - \frac{6k_B T}{W_M - k_B T \ln\left(\frac{1}{\omega\tau_0}\right)} \quad (4)$$

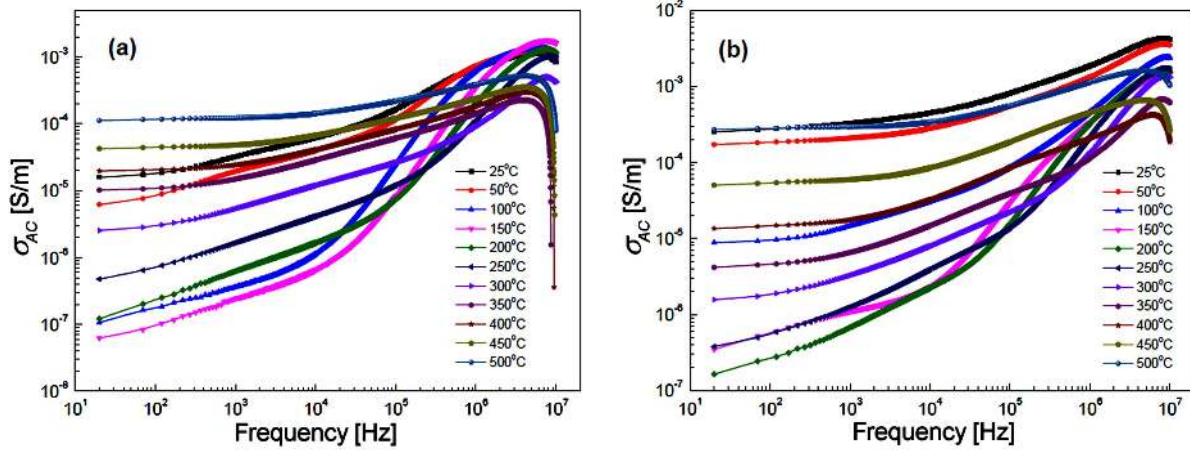


Figure 10. Frequency dependence of AC conductivity of: a) NT-0 and b) NT-10 NaTaO₃ ceramic samples at different temperatures

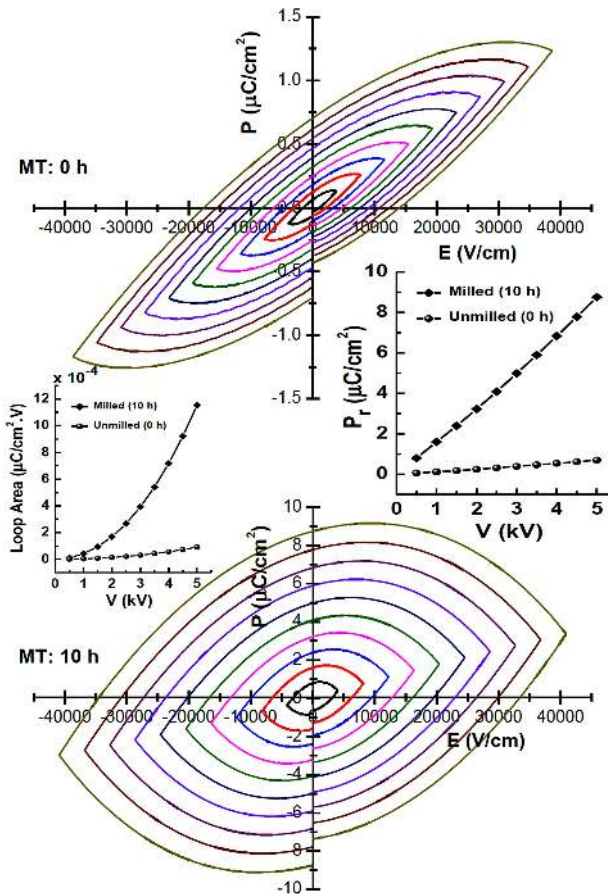


Figure 11. $P - E$ loops at room temperature and increasing fields of poled NT-0 and NT-10 ceramics prepared with unmilled (upper) and 10 h milled (lower) powders. Inset: Variation of P_r and loop area with applied voltage

where, W_M is the energy required to cross the barrier height, which predicts a decrease in the value of the index ‘ s ’ with the increase in temperature, it is found to be consistent with the experimental results. Therefore, the conduction in both the systems could be considered due to the short-range translational type hopping of charge carriers [7].

3.4. Ferroelectric properties

Figure 11 shows the electric field-induced polarization hysteresis ($P - E$) loops of the poled NT-0 and NT-10 ceramics measured at room temperature and different voltage levels. $P - E$ plots exhibit a typical ferroelectric hysteresis loop similar to such system. The values of remnant polarization P_r and coercive field E_c are observed to be $0.71 \mu\text{C}/\text{cm}^2$ and $2.03 \text{ kV}/\text{cm}$ for the poled NT-0 ceramics while these values were found to be $8.74 \mu\text{C}/\text{cm}^2$ and $4.14 \text{ kV}/\text{cm}$ for the NT-10 sample. Further, the $P - E$ loops are not very slim which may probably be due to slightly high leakage currents as can be seen from the round angle of the $P - E$ loops near to the maximum electric field. Also, it can be seen that the values of P_r and area of loops increase with increasing voltage and the values are always found higher for the ceramic prepared with milled NT powder (inset of Fig. 11).

IV. Conclusions

Polycrystalline NaTaO₃ ceramics, prepared by a high temperature solid state reaction route and high energy milling with different milling hours, were found to possess a perovskite type orthorhombic structure with the space group $Pnma$. FTIR spectra also confirmed the formation of NT without any new phase. The NT ceramics showed the formation of small grain sizes ($\sim 1.2 \mu\text{m}$) which is beneficial for dielectric applications in high density integrated devices. The NT ceramics prepared with 10 h milled powder exhibited superior dielectric properties (enhancement in ϵ' -value and reduction in $\text{tg } \delta$ -value) compared to the NT ceramics prepared with unmilled powder. Impedance analysis indicated the negative temperature coefficient of resistance character with non-Debye type of dielectric relaxation. The correlated barrier hopping model is found to successfully explain the mechanism of charge transport in present ceramic samples. The values of remnant polarization and coercive field of the poled NT ceramics prepared with unmilled and 10 h milled powders were found to

be $0.71 \mu\text{C}/\text{cm}^2$ and $2.03 \text{ kV}/\text{cm}$ and $8.74 \mu\text{C}/\text{cm}^2$ and $4.14 \text{ kV}/\text{cm}$, respectively. In summary, proper high energy milling of such electroceramic led to have multi-fold benefits such as improvement in homogeneity, reduction in particle as well as grain sizes and show superior dielectric properties.

References

- I.-T. Seo, C.-H. Choi, D. Song, M.-S. Jang, B.-Y. Kim, S. Nahm, Y.-S. Kim, T.-H. Sung, H.-C. Song, "Piezoelectric properties of lead-free piezoelectric ceramics and their energy harvester characteristics", *J. Am. Ceram. Soc.*, **96** (2013) 1024–1028.
- H. Du, Y. Huang, H. Tang, H. Qin, W. Feng, "Dielectric and piezoelectric properties of SrZrO₃-modified (K_{0.45}Na_{0.51}Li_{0.04})(Nb_{0.90}Ta_{0.04}Sb_{0.06})O₃ lead-free piezoceramics", *Mater. Lett.*, **106** (2013) 141–144.
- H. Du, Y. Huang, H. Tang, W. Feng, H. Qin, X. Lu, "Structure and electrical properties of [(K_{0.49}Na_{0.51})_{1-x}Li_x](Nb_{0.90}Ta_{0.04}Sb_{0.06})O₃ lead-free piezoceramics", *Ceram. Int.*, **39** (2013) 5689–5694.
- X. Vendrell, J.E. García, F. Rubio-Marcos, D.A. Ochoa, L. Mestres, J.F. Fernández, "Exploring different sintering atmospheres to reduce nonlinear response of modified KNN piezoceramics", *J. Euro. Ceram. Soc.*, **33** (2013) 825–831.
- S. Bhagat, K. AmarNath, K.P. Chandra, R.K. Singh, A.R. Kulkarni, K. Prasad, "The structural, electrical and magnetic properties of perovskite (1-x)Ba(Fe_{1/2}Nb_{1/2})O₃-xBaTiO₃ ceramics", *Adv. Mater. Lett.*, **5** (2014) 117–121.
- K. Prasad, Priyanka, K. AmarNath, K.P. Chandra, A.R. Kulkarni, "Dielectric relaxation in Ba(Y_{1/2}Nb_{1/2})O₃-BaTiO₃ ceramics", *J. Mater. Sci.: Mater. Electron.*, **25** (2014) 4856–4866.
- K. AmarNath, K. Prasad, "Structural and electric properties of perovskite Ba(Sm_{1/2}Nb_{1/2})O₃-BaTiO₃ ceramic", *Adv. Mater. Res.*, **1** (2012) 115–128.
- K. Kumari, A. Prasad, K. Prasad, "Structural and dielectric properties of ZnO added (Na_{1/2}Bi_{1/2})TiO₃ ceramic", *J. Mater. Sci. Technol.*, **27** (2011) 213–217.
- R.-A. Eichel, H. Kungl, "Recent developments and future perspectives of lead-free ferroelectrics", *Funct. Mater. Lett.*, **3** (2010) 1–4.
- D. Damjanovic, N. Klein, J. Li, V. Porokhonsky, "What can be expected from lead-free piezoelectric materials?", *Funct. Mater. Lett.*, **3** (2010) 5–13.
- P.K. Panda, "Review: environmental friendly lead-free piezoelectric materials", *J. Mater. Sci.*, **44** (2009) 5049–5062.
- J. Rödel, W. Jo, K.T.P. Seifert, E.-M. Anton, T. Granzow, D. Damjanovic, "Perspective on the development of lead-free piezoceramics", *J. Am. Ceram. Soc.*, **92** (2009) 1153–1177.
- W. Wunderlich, "NaTaO₃ composite ceramics - A new thermoelectric material for energy generation", *J. Nuclear Mater.*, **389** (2009) 57–61.
- T.R. Shrout, S.J. Zhang, "Lead-free piezoelectric ceramics: Alternatives for PZT?", *J. Electroceram.*, **19** (2007) 111–124.
- T. Takenaka, H. Nagata, "Current status and prospects of lead-free piezoelectric ceramics", *J. Eur. Ceram. Soc.*, **25** (2005) 2693–2700.
- X.M. Chen, Y.T. Lu, D.Z. Jin, X.Q. Liu, "Dielectric and ferroelectric characterization of Na(Ta,Nb)O₃ solid solution ceramics", *J. Electroceram.*, **15** (2005) 21–26.
- B.J. Kennedy, A.K. Prodjosantoso, C.J. Howard, "Powder neutron diffraction study of the high temperature phase transitions in NaTaO₃", *J. Phys.: Condens. Matter*, **11** (1999) 6319–6328.
- H. Kishi, Y. Mizuno, H. Chazono, "Base-metal electrode-multilayer ceramic capacitors: past, present and future perspectives", *Jpn. J. Appl. Phys.*, **42** (2003) 1–15.
- M. Cain, R. Morrell, "Nanostructured ceramics: a review of their potential", *Appl. Organometal. Chem.*, **15** (2001) 321–330.
- M.L.V. Mahesh, V.V. Bhanuprasad, A.R. James, "Enhanced piezoelectric properties and tunability of lead-free ceramics prepared by high-energy ball milling", *J. Electron. Mater.*, **42** (2013) 3547–3551.
- R. Zuo, J. Rödel, R. Chen, L. Li, "Sintering and electrical properties of lead-free Na_{0.5}K_{0.5}NbO₃ piezoelectric ceramics", *J. Am. Ceram. Soc.*, **89** (2006) 2010–2015.
- T. Rojac, Ž. Trtnik, M. Kosec, "Mechanochemical reactions in Na₂CO₃-M₂O₅ (M = V, Nb, Ta) powder mixtures: Influence of transition-metal oxide on reaction rate", *Solid State Ionics*, **190** (2011) 1–7.
- T. Rojac, P. Šegedin, M. Kosec, "Using infrared spectroscopy to identify new amorphous phases - A case study of carbonato complex formed by mechanochemical processing", pp. 13–42 in *Infrared Spectroscopy - Materials Science, Engineering and Technology*. Ed. T. Theophile, InTech, Croatia, 2012.
- S.K. Roy, S.N. Singh, K. Kumar, K. Prasad, "Structural, FTIR and ac conductivity studies of NaMeO₃ (Me ≡ Nb, Ta) ceramics", *Adv. Mater. Res.*, **2** (2013) 173–180.
- Y.M. Moustafa, K. El-Egili, "Infrared spectra of sodium phosphate glasses", *J. Non-Cryst. Solids*, **240** (1998) 144–153.
- A.K. Jha, K. Prasad, "Biological synthesis of cobalt ferrite nanoparticles", *Nanotechnol. Dev.*, **2:e9** (2012) 46–51.
- S. Kumar, L.K. Sahay, A.K. Jha, K. Prasad, "Synthesis of (Ag_{0.5}Fe_{0.5})TiO₃ nanocrystalline powders using stearic acid gel method", *Adv. Mater. Lett.*, **5** (2014) 67–70.
- K. Prasad, Lily, K. Kumari, K.P. Chandra, K.L. Yadav, S. Sen, "Electrical properties of a lead-free perovskite ceramic: (Na_{0.5}Sb_{0.5})TiO₃", *Appl. Phys. A*, **88** (2007) 377–383.

29. I. Molodetsky, P.K. Davies, “Effect of $\text{Ba}(\text{Y}_{1/2}\text{Nb}_{1/2})\text{O}_3$ and BaZrO_3 on the cation order and properties of $\text{Ba}(\text{Co}_{1/3}\text{Nb}_{2/3})\text{O}_3$ microwave ceramics”, *J. Eur. Ceram. Soc.*, **21** (2001) 2587–2591.
30. K. Prasad, S. Bhagat, Priyanka, K. AmarNath, K.P. Chandra, A.R. Kulkarni, “Electrical properties of $\text{BaY}_{0.5}\text{Nb}_{0.5}\text{O}_3$ ceramic: Impedance spectroscopy analysis”, *Phys. B: Condens. Matter*, **405** (2010) 3564–3571.
31. L.A. Khalam, H. Sreemoolanathan, R. Ratheesh, P. Mohanan, M.T. Sebastian, “Preparation, characterization and microwave dielectric properties of $\text{Ba}(\text{B}'_{1/2}\text{Nb}_{1/2})\text{O}_3$ [$\text{B}' = \text{La, Pr, Nd, Sm, Eu, Gd, Tb, Dy, Ho, Y, Yb}$ and In] ceramics”, *Mater. Sci. Eng. B*, **107** (2004) 264–270.
32. M.A.L. Nobre, S. Lanfredi, “Dielectric spectroscopy on $\text{Bi}_3\text{Zn}_2\text{Sb}_3\text{O}_{14}$ ceramic: an approach based on the complex impedance”, *J. Phys. Chem. Solids*, **64** (2003) 2457–2464.
33. R. Mizaras, M. Takashige, J. Banys, S. Kojima, J. Grigas, S.-I. Hamazaki, A. Brilingas, “Dielectric relaxation in $\text{Ba}_2\text{NaNb}_{5(1-x)}\text{Ta}_{5x}\text{O}_{15}$ single crystals”, *J. Phys. Soc. Jpn.*, **66** (1997) 2881–2885.
34. A.K. Jonscher, *Dielectric Relaxation in Solids*, Chelsea, New York, 1983.